Instability of Partial Cavitation: A Numerical/Experimental Approach

R.E.A.. Arndt[1], C.C.S. Song[1], M. Kjeldsen[2]., A. Keller[3]
([1]Saint Anthony Falls Laboratory, University of Minnesota, [2]Norwegian University of Science and Technology, [3]Technical University of Munich)

ABSTRACT

Sheet cavitation and the transition to cloud cavitation on hydrofoils and marine propellers results in a highly unstable flow that can induce significant fluctuations in lift, thrust and torque. In order to gain a better understanding of the complex physics involved, an integrated numerical/experimental investigation was carried out. A 2D NACA 0015 hydrofoil was selected for study, because of its previous use by several investigators around the world. The simulation methodology is based on large eddy simulation (LES), using a barotropic phase model to couple the continuity and momentum equations. The complementary experiments were carried at two different scales in two different water tunnels. Tests at the Saint Anthony Falls Laboratory (SAFL) were carried out in a 19 cm square water tunnel and a geometrically scaled up series of tests were carried out in the 30 cm square water tunnel at the Versuchsanstalt für Wasserbau (VAO) in Obernach, Germany. The tests were designed to complement each other and to capitalize on the special features of each facility.

INTRODUCTION

Marine propellers and hydrofoils must often operate in the cavitating regime. Various types of cavitation can be found in practice, including bubble cavitation, sheet cavitation, cloud cavitation, vortex tube cavitation and vortex sheet cavitation, depending upon how the low pressure regions are generated. In spite of considerable research, there are still many features of the problem that have not been properly explored. For example, inception studies are based on fully wetted flow properties, i.e. pressure distribution, turbulence level etc. in the absence of cavitation. On the other hand, classical models of developed cavitation consider only cavitation number as the primary variable. What has not been given adequate attention is a class of partially cavitating flows *in which there is an interaction between fluid turbulence and cavitation.* For example, vortex generation at the trailing edge of sheet cavitation is a manifestation of the cavitation itself (Ye et al, 1997). This is an important finding since turbulence is normally attributed to being a factor in the inception process, but cavitation as a mechanism for turbulence generation has been given scant attention.

Cavitation is also known to produce air bubbles due to incondensible gas coming out of solution in low pressure (supersaturated) regions of the flow. The production of bubbly flows in hydraulic equipment can have insidious effects on the stability of operation and on vibration. There are a variety of references in the literature to the interrelation between cavitation performance and dissolved air dating back as early as 50 years ago. However, a *quantitative* understanding of the interrelation between dissolved gas and cavitation phenomena is still beyond our grasp.

A particularly important form of cavitation from a technical point of view is attached cavitation on the surface of lifting surfaces. At typical angles of attack, this takes the form of a sheet, often terminated at the trailing edge by a highly dynamic form of cloud cavitation. Vortex cavitation is often observed in the cloud which is caused by vorticity shed into the flow field. These cavitating micro-structures are highly energetic and are responsible for significant levels of noise and erosion. Laboratory experimentation indicates that a variety of cavitating flow patterns are possible within the sigma-angle of attack (σ-α) plane (Kjeldsen, et al, 1999).

In spite of many excellent studies, the details concerning the transition of sheet cavitation to cloud cavitation is still not understood. From a design point of view, cavitating flows must be modeled over a given performance envelope in the σ-α plane in order to

accurately predict performance at off-design conditions and to assess the potential for noise and erosion. This requirement is still far from being realized at the present time. For example, it is well known that the modeling of partial, time-averaged cavities is not simple, due to the inverse character of the flow representation in the vicinity of the cavity and its wake. In addition, partial cavity models cannot explain the breakup of sheet cavitation at the trailing edge into detached cavitation clouds. The process is inherently unsteady even for steady free stream conditions. Within a certain envelope of σ and α the process is also periodic (Kjeldsen, et al,1999). This creates a modulation of the trailing cloud cavitation that is highly erosive and very noisy (Arndt et al,1997).

Although considerable research has gone into avoiding cavitation, little effort has been made to understand the complex physics associated with operation in the partially cavitating regime. The occurrence of sheet cavitation and the transition to cloud cavitation results in a highly unstable flow that can induce significant fluctuations in lift, thrust and torque. In order to gain a better understanding of the complex physics involved, an integrated numerical/experimental approach was used. A 2D NACA 0015 hydrofoil was selected for study, because of its previous use by several investigators around the world. The simulation methodology is based on large eddy simulation (LES), using a barotropic phase model to couple the continuity and momentum equations. These simulations were carried out in an interactive way with the experimental efforts. For example, early simulations indicated that pressure side cavitation can occur under special conditions. This was experimentally confirmed and has led to an exhaustive investigation of cavitation induced lift oscillations.

The LES approach was adopted to resolve space wise variation of the flow due to large scale eddies. The weakly compressible flow approach proposed by Song and Yuan (1988) is used to resolve the rapidly changing flows in the liquid phase and, at the same time, to speed up the computation as compared with a typical incompressible flow approach. To overcome the difficulty presented by the unsteady and multiple free surfaces, Kubota et al (1992) proposed a "bubble two-phase flow model" based on an assumption that the fluid consists of a bubble-water mixture and the bubble volume change is governed by a modified Rayleigh-Plesset equation. More recently Song et al (1997) assumed the fluid to be barotropic and the density is a continuos function of pressure in the entire liquid-vapor phase.

The pioneering works of Helmholtz (1868) and Kirchhoff (1869) assumed the cavitating flow to be a steady state free-surface potential flow of the ideal fluid. They completely ignored the dynamics of the gas flow and neglected the viscosity and compressibility of the liquid phase. An obvious penalty of neglecting viscosity is the inability to simulate flows having strong velocity gradient. Less known fact is that the compressibility effect is important if pressure changes rapidly with time, even when Mach number is very small (see Song, 1996). By ignoring gas dynamics, the numerical treatment of free surface boundary may become untenable for highly unsteady and multiple cavity cases. Unsteady cavity flows about hydrofoils are time wise and space wise highly variable two-phase flows, making it necessary to account for compressibility, viscosity as well as the gas dynamics.

The experiments were carried at two different scales in two different water tunnels, at the Saint Anthony Falls Laboratory (SAFL) and at the Versuchsanstalt für Wasserbau (VAO) in Obernach, Germany. The tests were designed to complement each other and to capitalize on the special features of each facility.

THEORETICAL CONSIDERATIONS

Compressibility boundary layer theory

The importance of compressibility in small Mach number flows has long been overlooked. It is generally known that the compressibility effect is negligible if the flow is steady and Mach number is small, $\mathbf{M} \leq 0.2$. However, Song (1996) has shown that the compressibility can't be ignored if the flow is highly unsteady even when M is very small. The equation of state of water in liquid phase can be accurately represented by the following equation for a very wide range of pressure change.

$$p - p_o = a_o^2 (\rho - \rho_o) \qquad \textbf{(1)}$$

In the above equation "a" is the sound speed and the subscript "o" represents a reference condition. By eliminating ρ from the equation of continuity using Eq.1 the following equation is obtained.

$$\frac{\partial \rho}{\partial t} + \overline{V} \cdot \nabla p + \rho_o^2 \nabla \cdot \overline{V} = 0 \qquad \textbf{(2)}$$

The second term of Eq.2 is proportional to M^2 and

negligible when M is small. But the first term can't be neglected if the pressure changes rapidly with time. This situation is analogous to the case that some viscous terms in the equation of motion need to be retained in viscous boundary layers of high Reynolds number flows. The following equation of continuity for weakly compressible flow is obtained by dropping the second term:

$$\frac{\partial \rho}{\partial t} + \rho_o a_o^2 \nabla \cdot \overline{V} = 0 \qquad \textbf{(3)}$$

For an incompressible fluid $a_o \Rightarrow \infty$ and the equation reduces to the following classic equation.

$$\nabla \cdot \overline{V} = 0 \qquad \textbf{(4)}$$

Eq.3 is valid as long as M is small but Eq.4 is valid only when M is small and the flow is not highly unsteady.

Using the impulsively started flow about a circular cylinder as an example, Song (1996) showed that the weakly compressible flow equations, Eq.3 plus the equations of motion of an incompressible fluid, gives the solution for the entire flow development process. The flow is transient and compressibility dominates during an initial time period of δ, which is called the compressibility (time) boundary layer thickness. It is defined as the time required for the steady flow to be 99 % established. For non-viscous fluids, the fully established flow is the steady incompressible flow, which is independent of a_o assigned in the computation. For a cylinder of diameter D in an infinite domain, the compressibility boundary layer thickness, δ, was determined, numerically as well as theoretically, to be

$$\frac{\delta U}{D} = 5M \qquad \textbf{(5)}$$

where U is the ambient velocity. In other words, the weakly compressible flow equations contain the hydraulic transient flow solution, which continuously evolves into the steady incompressible flow. While the transient flow is compressibility dependent the converged outer solution is independent of compressibility or M. Eq.5 also implies that the steady flow is 99% established when the starting pressure wave travels 5D distance away from the cylinder. But, if the cylinder changes its velocity within $\delta = 5\ D/a$, then the compressibility affects the flow all the time.

Song and Chen (1996) further analyzed the same impulsively started flow problem for the case of viscous fluid at modest Reynolds number. In this case the time required for the regular vortex-shedding flow to be established is much greater than δ , because the speeds of convection and diffusion are much smaller than the sound speed for small M flow. The outer solution or the established flow is an unsteady vortex shedding flow of essentially incompressible fluid except that there is also an acoustic component in the solution. The acoustic component is relatively weak and can be filtered out to yield the purely hydrodynamic solution. It was shown that the solution is identical to the solution of the incompressible flow equations in every detail, both space wise and time wise. But more importantly, the outer solution is independent of M assumed during the solution process. Thus, it is possible to select an arbitrarily large M to speed up the computation. It was shown that, by using M = 0.4, the speed of computation was about 100 times that of the best incompressible flow method known to the authors.

A single -phase flow approach for cavitating flows

A cavitating flow contains the liquid phase, which is essentially incompressible and the gas phase, which is highly compressible. Cavitation is such a violent phenomenon due to radical density change around the critical pressure, its full resolution is not practical. The method proposed herein is to regard the liquid-vapor as a single-phase fluid whose equation of state may be approximated by a continuous function which is linear in the liquid phase but non-linear in the gas phase. Consistent with the weakly compressible flow approach, Eq.1 is used when the pressure is above the critical value, p_c. This equation is joined smoothly at the critical pressure by

$$p = \sum A_i \rho^i \qquad for \quad p_\varepsilon \le p \le p_c \qquad (6)$$

and joined by the following equation at the lower end:

$$p = B\rho, \quad for \quad 0 \le p \le p_\varepsilon \qquad (7)$$

The coefficients are so adjusted that the resulting pressure-density curve has a desirable shape.

The equations of continuity and motion may be

written in a conservative form as follows.

$$\frac{\partial U}{\partial t} + \nabla\cdot\overline{F} = S, \qquad \overline{F} = iE + jF + kG \tag{8}$$

where S is a source, which may or may not exist and i, j, k are the unit vectors in x, y, and z directions, respectively. The functions U, E, F, G and S are defined in the following.

$$U = [p,\ \rho u,\ \rho v,\ \rho w]^T \tag{9}$$

$$E = [\rho a^2 u,\ \rho u^2 + p - \tau_{xx},\ \rho uv - \tau_{xy},\ \rho uw - \tau_{xz}]^T \tag{10}$$

$$F = [\rho a^2 v,\ \rho uv - \tau_{xy},\ \rho v^2 + p - \tau_{yy},\ \rho vw - \tau_{yz}]^T \tag{11}$$

$$G = [\rho a^2 w,\ \rho uw - \tau_{xz},\ \rho vw - \tau_{yz},\ \rho w^2 + p - \tau_{zz}] \tag{12}$$

$$S = [\rho\overline{V}\cdot\nabla a^2,\ 0,\ 0,\ 0]^T \tag{13}$$

The source term S is identically equal to zero for the liquid phase.

Numerical Approach

The finite volume approach with MacCormack's (1969) predictor-corrector method has been used with good results. Eq. 2 is first averaged over a computational finite volume. In the process, the volume integral of divergence is converted to the surface integral by applying the divergence theory. The resulting equation is

$$\frac{\partial\overline{U}}{\partial t} + \frac{1}{\Delta V}\int_{\Delta A}\underline{F}\cdot\underline{n}\ dA = \overline{S} \tag{14}$$

In the above equation the superscript bar means volume averaged quantity, A is the surface area, and $\underline{n}$ is the unit normal vector on the surface of integration. Since the quantities to be calculated are always the volume averaged values, the superscript bar will be dropped hereafter. The above equation is a simple statement of the law of conservation that the rate of increase of U in a volume is equal to the net influx of $\overline{F}$ plus the source S. Thus, Eq.14 can be discretized with any standard finite difference scheme. Yuan (1986) describes detailed description of the process used herein.

Since a finite volume approach can resolve only the quantity of scale larger than the finite volume used, it is necessary to use a closure model for turbulent flow simulation. A simple Smagorinsky (1963) subgrid scale turbulence model is used. This model assumes that the shear stress tensor τ_{ij} can be calculated by adding an eddy viscosity ν_t to the kinematic viscosity ν. Smagorinsky proposed the following equation for the eddy viscosity.

$$\nu_t = \frac{1}{2}(C\Delta)^2\left|\frac{\partial u_i}{\partial x_j} + \frac{\partial u_j}{\partial x_i}\right| \tag{15}$$

In the above equation C is a coefficient to be determined and Δ is size of the finite volume. Experience indicates that a C distribution, which is 0 on the wall and increases to 0.12 outside of the viscous boundary layer generally gives satisfactory results.

The size of finite volume used is often too large to adequately resolve the sharp velocity gradient near a solid wall where the viscous boundary layer is thin. For this reason a wall function or a partial-slip condition (becomes no-slip when boundary layer is thick) is used: see He and Song (1991) for a description of this condition. Because cavity is assumed to be a continuous extension of the liquid, no free surface boundary condition is necessary. Only the hydrodynamic quantities are of interest (acoustics are ignored) and, therefore, an arbitrarily large value of M=0.4 is chosen for the liquid part of the flow to speed up the computation. Recall that the outer solution of the weakly compressible flow equations is independent of M and represent the incompressible flow. Although much larger M can be used, the gain in computational speed diminishes as M is further increased.

EXPERIMENTAL METHOD

In order to gain a better understanding of the complex physics involved, a simple geometry was studied. A 2D NACA 0015 hydrofoil was selected because of its previous use by several investigators around the world. The experiments were carried out at two different scales in two different water tunnels. Tests

at SAFL were made in a 19 cm square high speed water tunnel. A complementary set of tests using a geometrically similar configuration was carried out in the 30 cm square water tunnel at the Versuchsanstalt für Wasserbau (VAO) in Obernach, Germany using a hydrofoil having a 128 mm chord length.

The SAFL test setup is shown in Figure 1. Because of the wide range of tests envisioned in the program, two identically shaped hydrofoils were used. One foil was mounted on a lift balance for force measurements. A second foil was highly instrumented with an array of static pressure ports and an array of piezoelectric film transducers, quartz crystal transducers, and miniature accelerometers. The SAFL facility was also equipped for acoustic studies, Laser Doppler Anemometry for the study of wake characteristics and Phase Doppler Anemometry for measure of bubble size distribution in the wake.

The larger foil used in the Obernach tests was mounted at each end in specially designed force balances utilizing Kistler quartz crystal sensors as shown in Figure 2. These force balances have very high frequency response (≥ 3 KHz), which was found to be an important factor in the success of the program.

LabView data acquisition software was used in both facilities. This allowed for compatibility of the data sets between the US and Germany. This was of immeasurable benefit in coordinating measurement activities at two different laboratories. from each facility. An added benefit was the ability to carry out on-line comparisons.

Measurements at Obernach were complemented with normal and high speed video at 4,500 frames per second. At the same time, observations at SAFL were made utilizing a 35 mm camera and strobe lighting triggered by specially conditioned pressure signals measured on the foil. By capturing a sequence of photos at different time delays, equivalent framing rates as high as 100,000 per second can be achieved.

LIFT OSCILLATIONS

Excellent agreement was obtained between the numerical simulations and the data obtained at SAFL and Obernach. As an example, the measured cavity length at various angles of attack is presented in Figure 3 in the form of l/c vs σ/2α. These data are compared with previously collected data for an NACA 0015 hydrofoil with an elliptic planform of aspect ratio 3 by Arndt et al

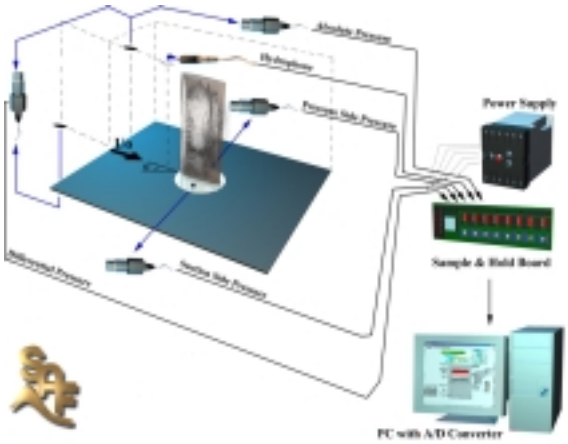

Figure 1. Schematic of sheet/cloud cavitation test set up in the SAFL High Speed Water tunnel.

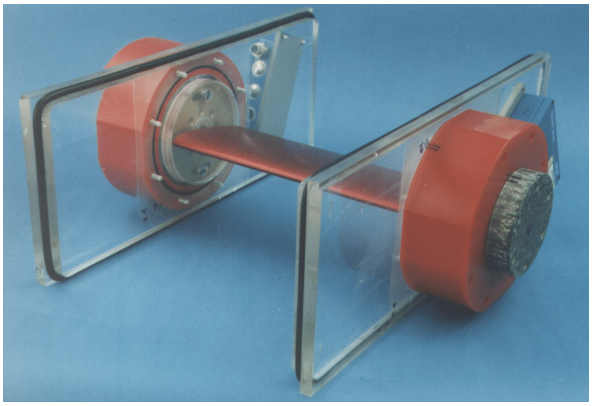

Figure 2. View of hydrofoil and lift balance setup at Obernach

(1997). The comparison is made by adjusting σ/2α for the 3D data to equivalent 2D values, using standard lift line theory. Also plotted is the partial and super-cavitation theory of Watanabe etal(1998)[1].

[1]Courtesy of Professor Watanabe who applied his cavitating flat plate theory to our test setup. The effects of blockage are apparently minimal since the theory agrees well with the theory of Acosta (1955) for an unconfined flat plate.

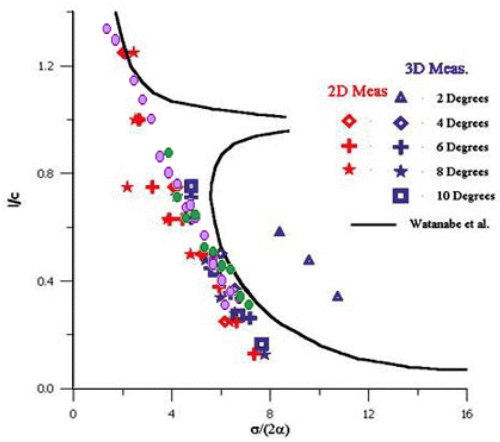

Figure 3. Cavity length data. The purple and green data are from the Obernach experiments.

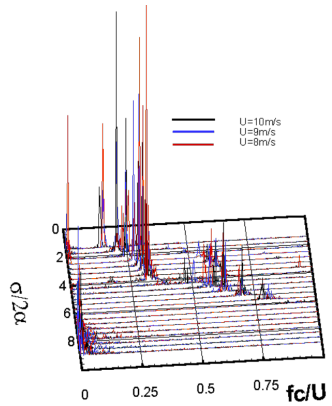

Figure 4. The measured lift oscillations for a cavitating hydrofoil have complex spectral characteristics. This is a collection a spectra collected over a range of cavitation number and flow velocity. The angle of attack, α, is 8 degrees. Very similar results occur at other angles of attack.

All the data agree except for the 2° data. The discrepancy at 2° is not unexpected since careful inspection indicates that bubble cavitation occurs at this angle of attack. Considering the assumptions made in the theory, the agreement with experiment is quite good. It is also noted that agreement between the 2D foil and the elliptic planform foil is quite satisfactory, suggesting that a quasi-2D theory might be a good estimate for cavity length for elliptically loaded foils.

The process was found to be highly dynamic. Cavitation induced lift oscillations have spectral characteristics that vary considerably over a range of $1.0 \le \sigma/2\alpha \le 8.5$, where σ is the cavitation number and α is the angle of attack, as shown in Figure 4. The amplitude of the fluctuations can exceed 100% of the steady state lift and are associated with the periodic shedding of vortical clouds of bubbles into the flow. Three types of oscillatory behavior are noted:

- $1.0 \le \sigma/2\alpha \le 4$: A strong spectral peak exists at a Strouhal number, fc/U, of about 0.15 that is independent of cavitation number.
- $4 \le \sigma/2\alpha \le 6$: A higher frequency, albeit weaker spectral peak dominates. The frequency of this peak is almost a linear function of cavitation number and corresponds to a constant Strouhal number, *based on cavity length,* of about 0.3.
- $6 \le \sigma/2\alpha \le 8.5$: Bubble/patch cavitation can occur. This induces a distinct, *very low frequency,* spectral peak.

The transition that occurs at $\sigma/2\alpha = 4$ corresponds to a relative cavity length, l/c, of about 0.75. This behavior is predicted by Watanabe et al (1998). They refer to type II modes as $l/c < 0.75$ and type I modes for $l/c > 0.75$.

The amplitude of the fluctuations can exceed 100% of the steady state lift and are associated with the periodic shedding of vortical clouds of bubbles into the flow. Amplitude data were normalized in the form:

$$Normalized\ Amplitude \equiv \frac{L_{rms}}{\pi\alpha\rho U^2 Sc} \qquad (16)$$

where L_{rms} is the root mean square lift, ρ is density, U is velocity , S is the span and c the chord length. Data obtained at two different scales with varying velocity and angle of attack were found to collapse very well. This is shown in Figures 5a and 5b.

Two competing mechanisms are found for the induced shedding of cloud cavitation. At high values of σ/2α, reentrant jet physics dominate, with sheet cavity oscillations at a frequency, based on cavity length, of $fl/U \approx 0.3$. At low values of σ/2α, bubbly flow shock wave phenomena dominate with a constant Strouhal number based on *chord length* of $fc/U \approx 0.2$. A significant effect on the wake structure is also noted.

Frequency data collected from high speed video of the flow are shown in Figure 6. These data agree very well with the lift data shown in Figure 4. Note that at approximately $\sigma/2\alpha \approx 4$, there is a sharp transition from

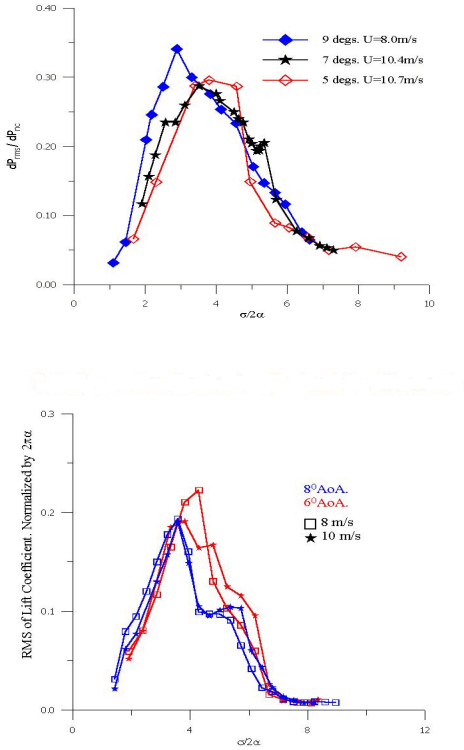

Figures 5a and b. Variation of rms lift with σ/2α. The upper figure is from the SAFL tunnel where lift is sensed by the pressure difference across the foil (Kjeldsen et al, 1999)

one type of frequency trend to the other. In fact, Joint Frequency Time Analysis (JTFA) clearly visualizes this process. This is shown in Figure 7. Lift spectra are shown for σ/2α= 3.82 and 3.34. In both cases there are two frequency peaks. At the higher value of σ/2α the higher frequency peak has a larger amplitude. At the lower value of σ/2αthe lower frequency peak has a larger amplitude. Only through the use of JTFA can it be found that both mechanisms do not occur simultaneously. As shown in figure7, when the lower frequency is dominant, it also occurs for a greater portion of time. When the higher frequency is dominant, it persists over a greater portion of time. This leads us to believe that two different mechanisms with different frequency characteristics are possible in this range of σ/2α.

COMPARISONS WITH SIMULATIONS

Bubble/Patch Cavitation

When the attack angle is small, the boundary layer of non-cavitating flow is thin and attached to the foil

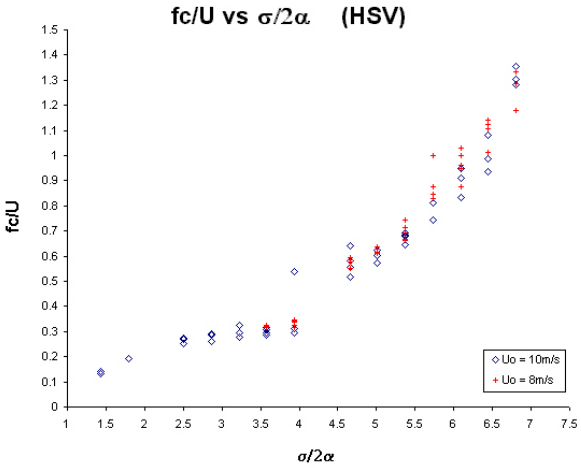

Figure 6 Measured frequency of oscillation from high speed videos. (VAO data)

every where except at the trailing edge. If the cavitation number is gradually decreased, then a bubble cavity will appear first near the nose where the pressure is minimum. The expansion due to bubble cavity induces boundary layer separation as indicated by an instantaneous vorticity field shown in Fig. 8. The corresponding pressure field shown in Fig. 9 indicates that the bubble is located at the middle of this large separation eddy. The computed pressure at three points on foil surface and lift coefficient as functions of time are shown in Fig. 10. The lift coefficient curve exhibit a saw-teeth form indicating that the time of bubble cavity formation coincides with the time of maximum lift. The bubble slides along the foil and collapsing near the trailing edge as the lift decreases to the minimum. As the collapsed cavity in the form of a large eddy is being transported in the wake, the boundary layer gradually recovers its original form and the lift increases to a maximum. A new bubble cavity is formed when the lift is maximum and the pressure is minimum again. The computed Strouhal number for this case is, S = fc/U = 0.1 which corresponds to Type 3 oscillations.

Sheet-Cloud Cavitation (partial cavitation)

In the midrange of σ/2α an attached sheet cavity will form near the nose. This cavity is highly unsteady; it periodically grows and breaks off to form a cloud cavity. Fig.11 shows vorticity fields at several instants within one cycle of vortex shedding or cloud cavity formation. This figure suggests that the cavity break off is due to the reentrant jet striking the cavity surface (reentrant jet is a thin positive vortex sheet). It also suggests that the cloud cavity is a large eddy

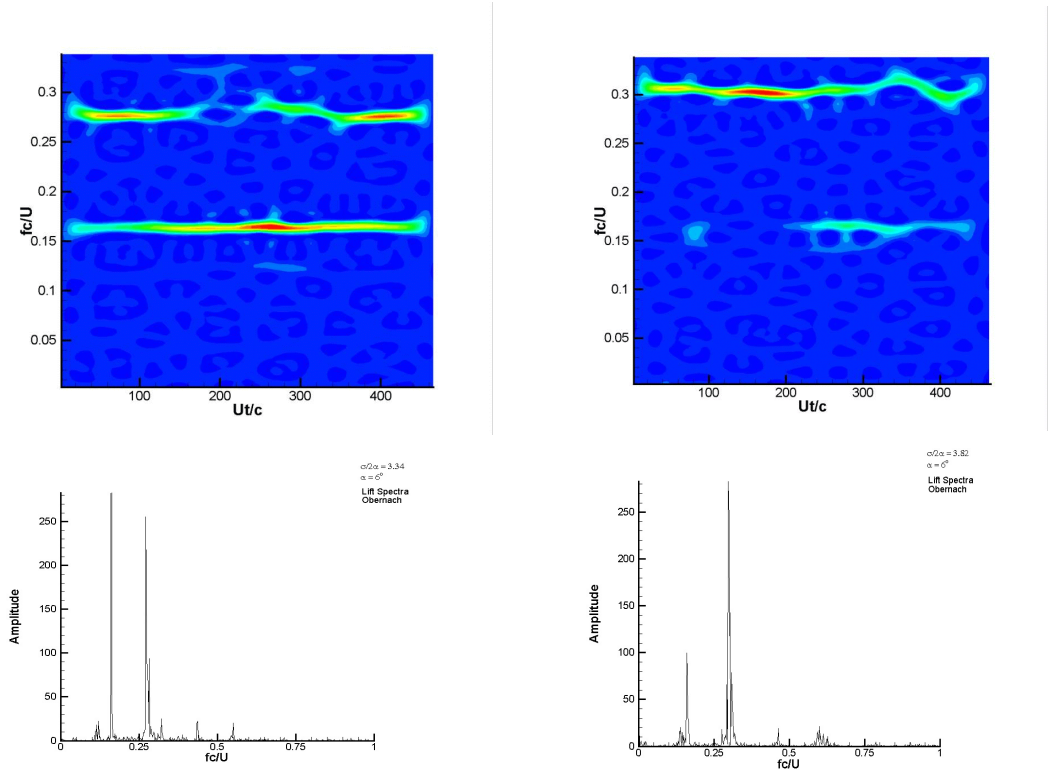

σ/2α = 3.34 σ/2α = 3.89

Figure 7. Comparison of conventional lift spectra and JTFA analyses for two values of σ/2α

containing many small eddies. Comparison with a phase locked photograph of the process indicates how well the simulation captures the essential physics of the process.

Typical computed vorticity, pressure and density fields at one instant are shown in Fig.12. This figure reveals, among other things, that a large number of bubble cavities reside inside the large shed vortex where pressure is low to form a cloud cavity. It is also interesting to note that the reentrant jet just broke the sheet cavity represents a high pressure zone, as to be expected. A short sheet cavity is located near the nose and a large non-cavitating vortex is located at mid-chord. The pressure field shown here is essentially the hydrodynamic pressure field that is transported mainly by convection. For the condition shown in Fig. 11 the sheet cavity breaks off near mid-chord and the cloud cavity collapses near the trailing edge.

Some typical spectrum of lift oscillation for at various cavitation numbers are shown in Fig.13. For the condition shown in Fig.11, there are two distinctive peaks in the spectrum. The first peak corresponds to the frequency of cloud cavity generating vortex shedding. As experiment has shown, this frequency is roughly inversely proportional to the cavity length. Fig. 13 also shows a second peak having twice the frequency of the first peak. The source of the second harmonic is not clear at this time, but may be due to the existence of the non-cavitating vortex shedding as shown in Fig. 12.

Sheet-Cloud Cavitation (full cavitation)

There is a significant change in the flow pattern when the maximum sheet cavity length exceeds the chord length. This is because the cavity terminates on the foil part of the time and terminates away from the foil the rest of the time. In other words, the cavity oscillates between partial cavity condition and supercavitating condition. Fig. 14 shows six instantaneous vorticity fields during one period of sheet/cloud cavitation. Observe that the sheet cavity start at the nose (see picture a) , grows to equal the chord length (see picture c), and eventually exceeds the chord (see pictures d and e). The super cavity terminates where the positive vorticity extending from the pressure side meets the negative vorticity that is the cavity surface on the suction side.

From picture (e) the maximum sheet cavity length

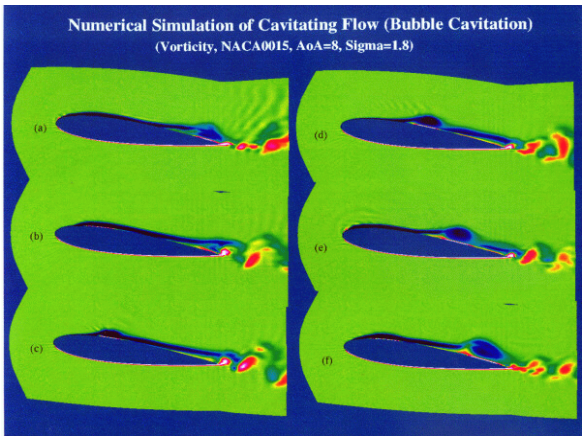

Figure 8. Vorticity field for bubble/patch cavitation, $\sigma/2\alpha = 6.44$

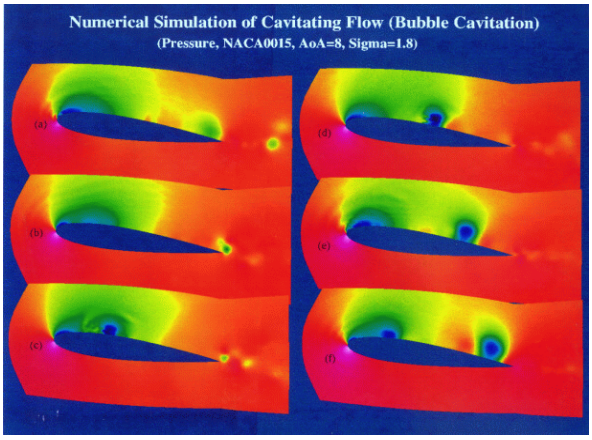

Figure 9 Pressure field during bubble/patch cavitation, $\sigma/2\alpha = 6.44$

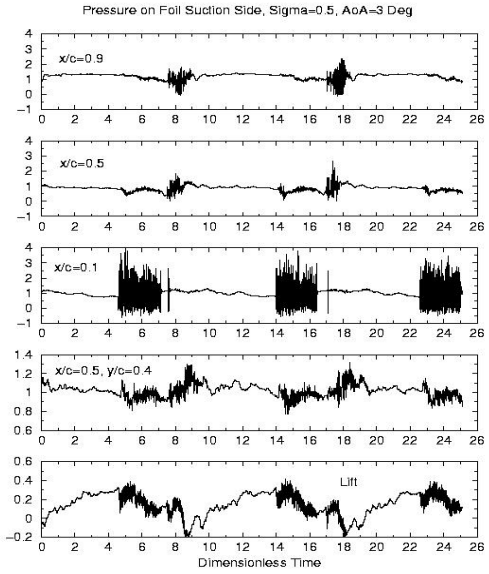

Figure 10. Numerical simulations of Type III oscillations due to bubble/patch cavitation. The lower curve displays lift fluctuations. The upper three curves are pressure at varius values of x/c.

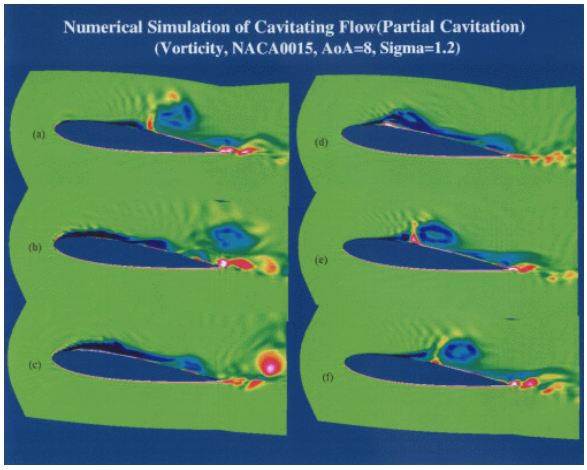

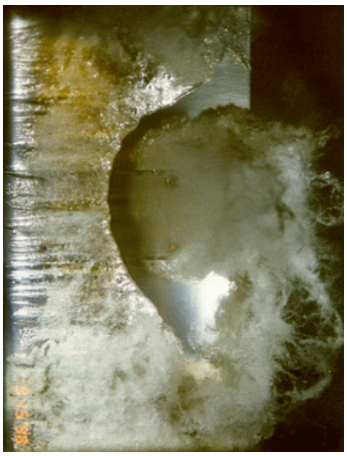

Figure 11. Numerical simulations at $\sigma/\alpha = 4.3$ are compared with a phase-locked photo of the process. Flow is from left to right. Shown is the variation over one cycle of oscillation. Red denotes positive vorticity.

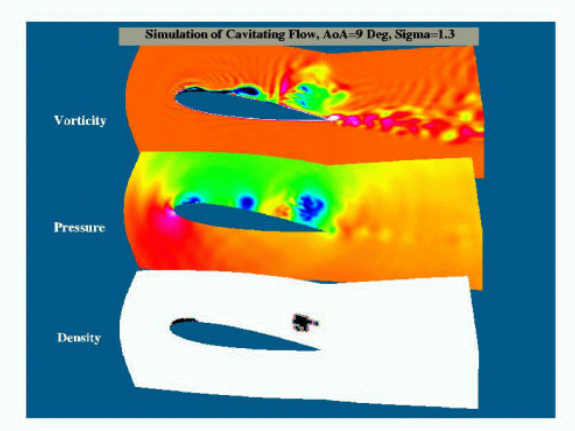

Figure 12 Simulation snapshot for σ/2α = 4.1

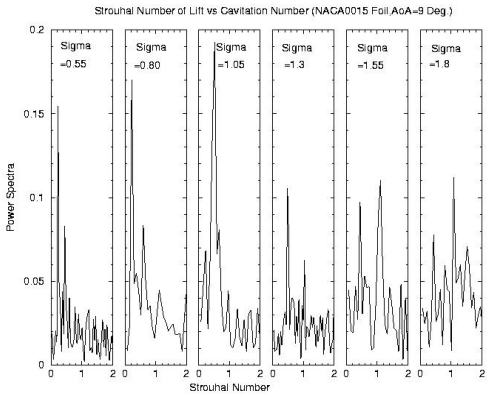

Figure 13. Computed variation in spectral characteristics with increasing σ. σ/2α varies from 1.75 to 5.73

is estimated to be about 1.3 c. This long sheet cavity is about to be broken off by the reentrant jet as shown by picture (e). Pictures (f,a,b) show the convection of the large eddy or the cloud cavity after it is broken off. The cloud cavity collapses further downstream, which is outside of the region shown in the figure. Fig. 15 is an illustration of the pressure field at the same time increments as for the vorticity. This figure also shows evidence of shock wave produced by the collapsing cloud cavity traveling upstream. As observed experimentally, the shock wave can destroy the sheet cavity near the nose for short period of time as shown by picture (f) of Figure 14 (very thin boundary layer indicates no cavitation.) This was a surprise when first observed experimentally.

In addition, Figure 13 shows that the lift oscillations also contain two peaks. In this case the primary peak is that of the sheet/ cloud cavity oscillation, which is dependent on the chord length rather than the cavity length. Also in agreement with experimental observations.

Wake Characteristics

Cavitation has a profound effect on the wake characteristics behind a hydrofoil. During the current study, LDV measurements were made in the wake of the foil in cavitating and non-cavitating conditions. Velocity profiles were obtained a several cross-sections downstream of the trailing edge of the foil. Mean velocity data were obtained and analyzed for a variety of conditions (σ and α). To date, two different types of analysis have been performed. These analyses provide not only insight into understanding the periodic

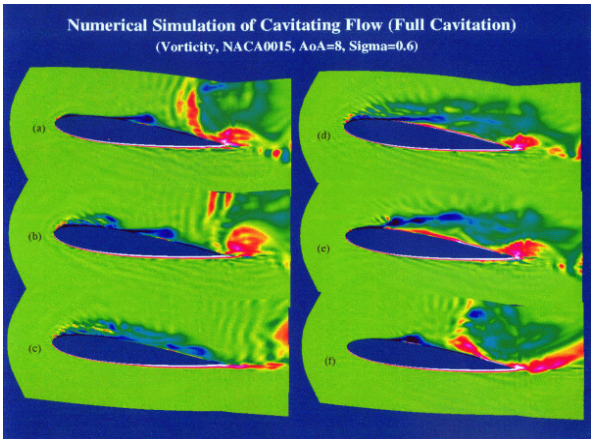

Figure 14. Computed vorticity field for σ/2α = 2.15

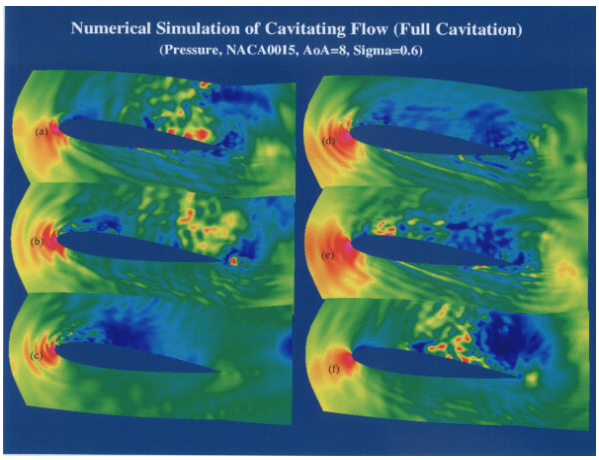

Figure 15. Numerical simulation of the pressure field during extensive cavitation, σ/2α = 2.15

phenomena cited above but also provide insight into the problem of predicting bubbly wakes due to cavitation. The basic idea for both methods is an observed increase in measured data rate when bubbles are passing through the LDV measurement volume. This increase is, in general, greater than 10 times that for non-cavitating conditions. The wake flow behind the hydrofoil was also investigated for both cavitating and non-cavitating conditions.

Using LDV measurements, it is found that self-similarity of the wake shape exists quite close to the trailing edge (x/c=0.12), for both cavitating and non-cavitating flow. Mean velocity profiles for cavitating and non-cavitating conditions are presented in Figure 16. The data are presented in a form suggested by the similitude of turbulent wakes:

$$\frac{(U_{ref} - u(y))}{U_{ref}}\sqrt{\frac{x}{c}} = f\left[\frac{y}{\sqrt{xc}}\right] \qquad (17)$$

where x is distance from the trailing edge, y is the distance normal to the flow measured from the center of the wake c is the chord length and U_{ref} is the velocity at the edge of the wake. It is clearly evident that the rate of spreading of the wake is significantly larger under cavitating flow conditions. This effect has been also reported by other workers in the field (Kubota et al, 1989). When cloud cavitation is present, large vortical structures containing numerous bubbles are observed to be shed into the wake. These clouds of bubbles extend much further in the cross stream direction than the viscous wake associated with non-cavitating flow.

Much of the important physics in the process are obscured by the averaging process. While the non-cavitating LDV signal resembles a typical turbulence signature, the cavitating signal is skewed towards lower velocity. The strong negative fluctuations in velocity are due to the imprint left by the periodic passage of vortices from the cavitation process that extends much further from the wake centerline than a typical viscous wake. This is graphically illustrated in the numerical simulations shown in Figure 11. In fact there is excellent agreement between animated simulations and high speed videos of the vortical clouds of bubbles.

The numerical simulations shown in Figure 11 are for a case close to the maximum amplitude of lift oscillations. Note the strong upwelling close to mid-span that results in strong oscillations in lift and surface pressure. It should also be pointed out that averaged

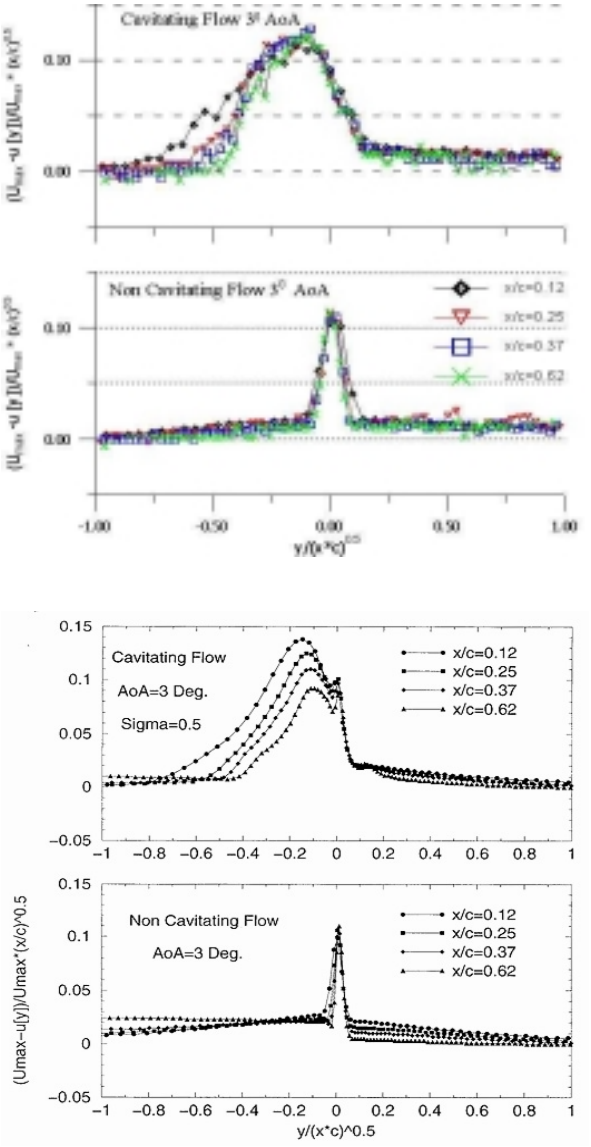

Figure 16 Experimental (above) and numerical (below) wake data with/without cavitation compared. y = 0 is taken to be that of maximum velocity deficit for the non-cavitating case.

numerical data also agree very well with the experimental data shown in Figure 16 for *both cavitating and non-cavitating flow.* In the case of cavitating flow, it is important to note that the numerical simulations fit the data close to the trailing edge, but deviate from the measurements further downstream. It is conjectured that this is an effect of dissolved gas that has come out of solution. The current numerical model considers only vapor that will condense downstream, while gas bubbles will persist in the wake.

It is also natural to conclude that the gas content in the wake will show a cyclic behavior. By also considering the fact that bubbles are counted more efficiently than naturally occurring LDV seeds in the flow, the average velocity will contain more weight from the shed bubbles. This has an effect on the LDV measurements that still needs to be resolved. However, the observation that the wake spreading is significantly more pronounced with cavitation is still qualitatively correct.

It was also found that a plot of data rate versus time could give additional information regarding cavitation dynamics. The data rate is defined as the time elapsed between two acquired valid samples by the LDV system. In general the best agreement is found for the two measurements in the intermediate domain between performance breakdown and super-cavitation. In comparing the LDV frequency domain fingerprint with the corresponding lift, similarities are found. This is shown in Figure 17.

It is noted that higher harmonics show up in both the spectra of the lift fluctuations and the data rate. It can be conjectured from the spectrum analysis and from inspection of the data rate time series alone, that the bubble shedding process occurs over a limited fraction of the total lift cycle. Since the lift and data rate spectra are similar, it can be inferred that the lift oscillations are also a result of the relatively rapid sheet cavity collapse process.

In concluding this section the following items are underscored:

- The LDV data rate is a useful diagnostic. Spectral analysis of these data indicate a link between the shedding of bubble clouds into the wake and the observed lift oscillations.
- The observed self similarity of the mean velocity data for both cavitating and non-cavitating conditions when compared with the numerical simulations suggest that dissolved incondensible gas plays an important role in the wake dynamics.
- In interpreting averaged velocity data from cavitating flows care must be taken because of the bias induced by slower moving bubble clouds that produce a higher than average data rate.

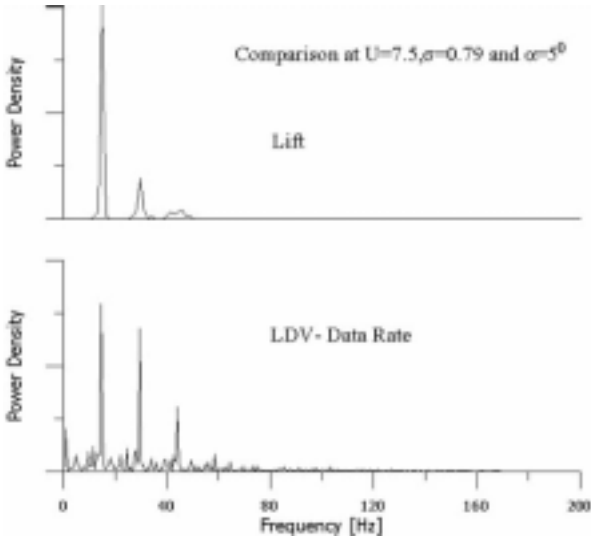

Figure 17. Comparison of lift dynamics with the FFT of data rate in a cavitating flow.

NOISE AND SURFACE PRESSURE CHARACTERISTICS

Surface pressure and noise data are additional diagnostics that provide further insight into this complex flow process. Figure 18 is a plot of surface pressure measured at various positions along the span of the foil. Note that the peak amplitude corresponds to about $\sigma/2\alpha = 3$ at about $x/c = 0.75$. This correlates well with the information displayed in Figure 11. The peak rms pressure is about 15 times the dynamic pressure. This value could be even higher because of size effects in piezoelectric film measurements (Arndt et al, 1997). As was already shown in Figure 5, the rms lift peaks at a slightly larger value of $\sigma/2\alpha$, but a direct comparison is not expected since the lift oscillations are due to the integrated effect of the pressure oscillations over the entire foil.

As would be expected, the spectral characteristics of the surface pressure in the region of maximum intensity should be similar the to the spectral characteristics of the surface pressure. This is shown in Figure 19 that is similar to Figure 4. Note that a similar bifurcation in the peak frequency occurs at about σ/2α = 4. In analogy with the lift data displayed in Figure 7, spectra at two values of σ/2α are shown for x/c = 0.74 are shown in Figure 20. Two dominant peaks are evident, with the higher frequency peak being dominate at the higher value of σ/2α. When comparing these spectra with JTFA analyses of the same data, it is also noted that either one frequency or the other occurs, but not simultaneously.

The duration of each frequency is proportional to the amplitude of that frequency component in the conventional spectrum. With lift oscillation and pressure data as a guide, the spectral characteristics of the noise can be analyzed The spectra are normalized in the following manner:

$$S\left(\frac{fc}{U}\right) \equiv \frac{\overline{p_a^2}}{\rho^2 U^4 \frac{\Delta f c}{U}} \qquad (17)$$

where $\overline{p_a^2}$ is the mean square acoustic pressure and Δf is the frequency bandwidth.

Noting that the spectral characteristics of the lift oscillations vary considerably with σ/2α, it is interesting to compare how the spectral characteristics of the noise vary over the same range. This is shown in Figure 21 where spectra at different values of σ/2α are compared over the same range shown in Figure 4 for lift oscillations. It is very clear that the noise maximizes in the same region as the lift oscillations are a maximum. The noise also persists to much higher frequencies.

COMPARISON WITH NON-CAVITATING SEPARATED FLOWS

Numerous experiments and numerical studies of flows over a foil in a non-cavitating condition have been carried out for several decades. The general flow patterns at different attack angles are well described based on both experiments and computations. For the purpose of comparison and for better understanding of the mechanics of cavity flows, this numerical model has also been used to simulate non-cavitating flows about NACA0015 foil. A non-cavitating condition is simulated by assigning a very large value to the

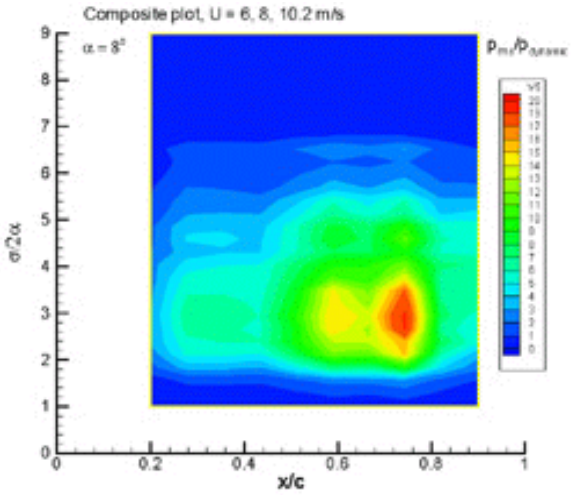

Figure 18. RMS surface pressure. The intensity of the color denotes the amplitude normalized to dynamic pressure.

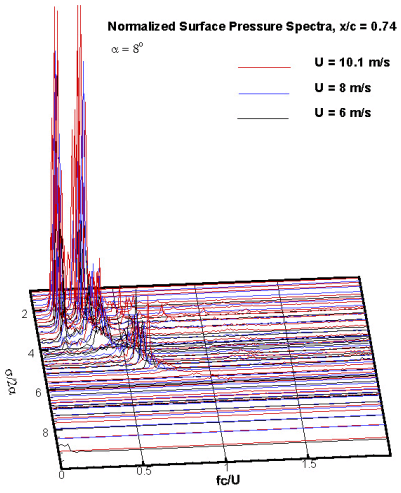

Figure 19. Surface pressure spectra at l/c = 0.74

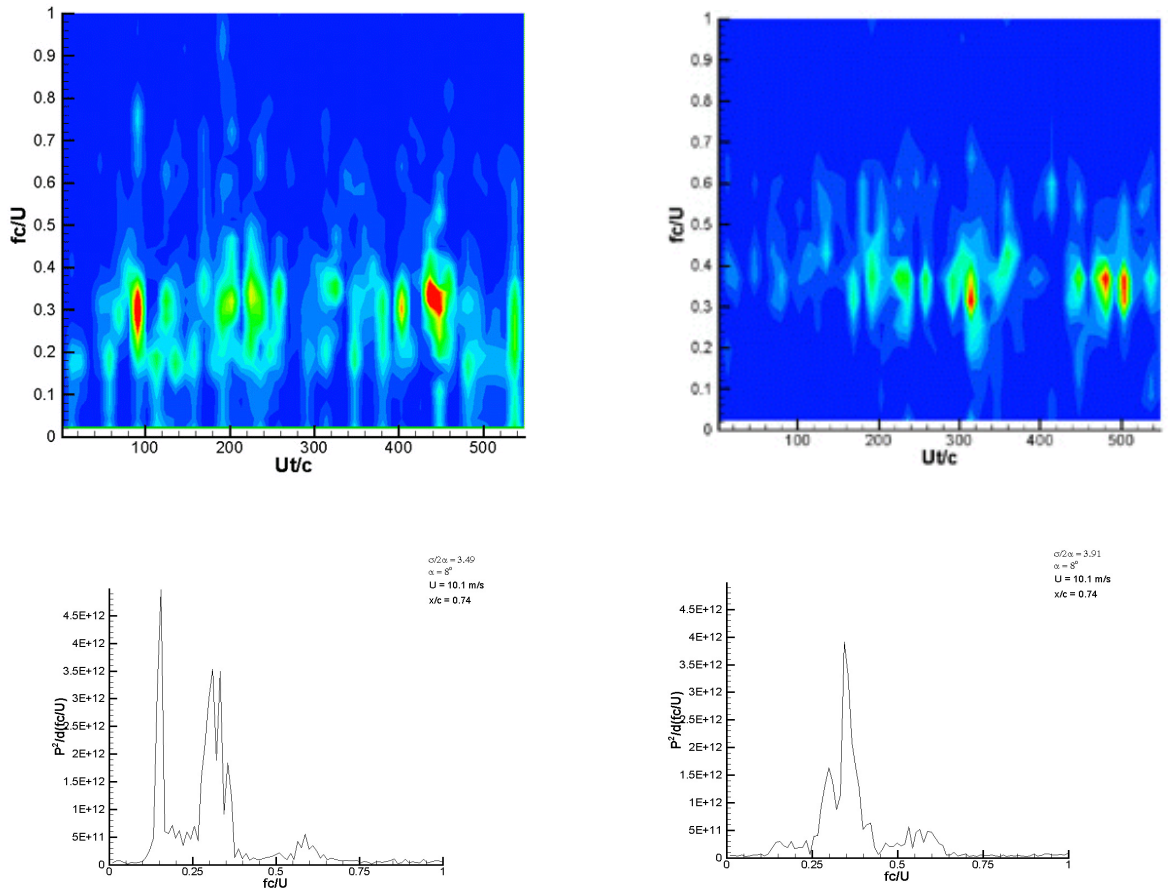

σ/2α = 3.49 σ/2α = 3.91

Figure 20. Spectral characteristics of surface pressure are compared at l/c = 0.74 for two values of σ/2α

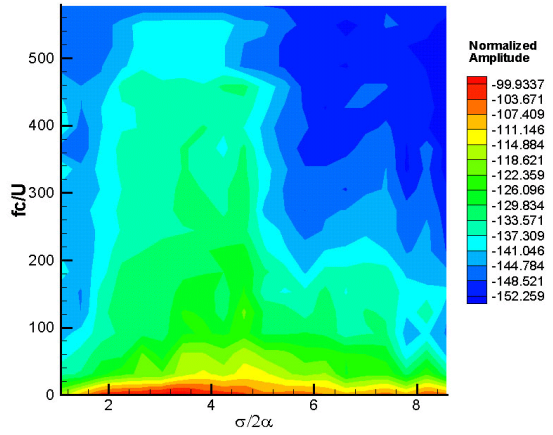

Figure 21 Spectral characteristics of radiated sound.

cavitation number while the Reynolds number is kept constant at 10^5. The boundary layer is fully attached when the angle of attack is small. Boundary layer separation occurs at about 90% chord when $\alpha = 8°$. The separation point creeps upstream as α is increased to $11°$ while the separated flow remains stable. The only oscillatory motion is that of the wake instability.

A slight increase of the angle of attack to $12°$ results in the separation point moving upstream to about 25% chord with vortex shedding taking place as shown in Fig. 22. The elongated separation bubble "a" detaches to produce a large clockwise rotating eddy "b" which convects downstream to become "c". When eddy "b" detaches from "a" it induces a counter rotating vortex "d". It is interesting to compare Fig. 22 with Fig.11 and find that there is much similarity between a cavitating flow and a non-cavitating flow at a somewhat larger attack angle. In both cases, the flow is dominated

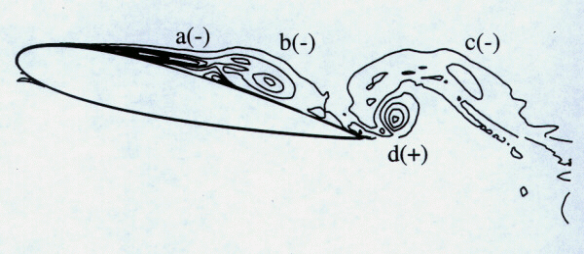

Figure 22. Simulation of non-cavitating flow at $\alpha = 12°$

by a periodic growth and detachment of a boundary layer separation bubble. The downstream part of the elongated separation bubble is a large coherent eddy dominated by negative vorticity. But there is a thin layer of positive vorticity near the foil surface shown in red. This reverse flow with positive vorticity is a reentrant jet that is responsible for the breaking away of the sheet cavity. The way that the reentrant jet terns upward and wraps around the detached large eddy can be observed in both cases.

SUMMARY AND CONCLUSIONS

An extensive investigation of sheet/cloud cavitation was carried out using both numerical and experimental techniques. Properly normalized, the data agree in both amplitude and spectral characteristics. Data for lift, surface pressure and noise are remarkably consistent. Three flow regimes are noted roughly demarcated by the parameter $\sigma/2\alpha$. A strong bifurcation in the data exists at $\sigma/2\alpha$ where the maximum amplitude in lift, noise and pressure is noted.

Excellent agreement with numerical simulations was achieved. This leads to a very optimistic view of the simulation model used. Steps have been taken to significantly reduce computation time. The authors feel that this combined numerical/experimental approach shows great promise for further research.

It is important to underscore the fact that $\sigma/2\alpha$ is a parameter whose genesis is found in *linearized inviscid* theory for a thin flat plate. It was a surprise that this parameter was even an approximate description of cavitating flow. Detailed examination does show that the vertical extent of the cavity flow is less at lower angle of attack even though l/c and $\sigma/2\alpha$ are constant.

The acoustic radiation from different cavitation patterns on a NACA 0015 hydrofoil were studied. In addition, the noise characteristics were correlated with measurements of unsteady pressure on the surface of the foil. These measurements were made using a new method utilizing piezoelectric film.

The noise characteristics are very similar to the characteristics of the lift oscillations. Numerical and experimental work have identified three regions of cavitating flow. Cavitation noise spectra were also found to vary significantly with the type of cavitation, e.g. bubble/patch, sheet/cloud or fully developed super-cavitation. The best correlating parameter is $\sigma/2\alpha$. This is parameter is only truly valid for a thin flat plate (Acosta, 1955). However even for the relatively thick foil studied here, the overall features of the flow are determined by this parameter.

The acoustic pressure peaks at about $\sigma/2\alpha$.= 3.5. The spectra persist to high values of frequency in the range $2.5 \le \sigma/2\alpha \le 5.0$. Reasonably good collapse of the data was found by normalizing in the form

$$\frac{p_a^2}{\frac{\Delta fc}{U}\rho^2 U^4} = f\left(\frac{fc}{U}\right)$$

The surface pressure technique shows good promise for detecting regions of intense cavitation activity. The observed pressure characteristics are in good qualitative agreement with the numerical simulations and the measured lift oscillations. The array of techniques developed to study this complex flow show good promise for surface pressure/acoustic radiation and lift/acoustic radiation correlations.

ACKNOWLEDGMENTS

This work was sponsored by the National Science Foundation and the Office of Naval Research. Mr Michael Levy provided invaluable assistance in obtaining the noise and pressure data. Mr. Fayi Zhou and Dr. G. Wang have also provided some help at the early stage of the program. The computer time has been provided by the Minnesota Supercomputer Institute, University of Minnesota through its grant program.

REFERENCES

Acosta, A.J. (1955) “A note on partial cavitation of flat plate hydrofoils” Calif. Inst. of Tech. Hydro Lab, Rep.E-19.9

Arndt, R. E. A. (1981), "Cavitation in fluid machinery and hydraulic structures", Ann. Rev. Fluid Mech.,

Vol. 13.

Arndt, R.E.A., Voigt, R. L. Jr., Sinclair, J., Rodrigue, P., and Ferreira, A, (1989) "Cavitation Erosion in Hydroturbines,", *Journal of Hydraulic Engineering*, ASCE, October

Arndt, R.E.A., Paul, S and Ellis, C.R. (1997) "Application of piezoelectric film in cavitation research" Journal of Hydraulic Engineering, Vol. 123, no. 6, June

Doligalski, T. L., Smith, C. R., and Walker, J. D. A., 1994, "Vortex interactions with walls," Ann. Rev. Fluid Mech., vol. 26, pp. 573-616.

Helmholtz, H. (1868), " On Discontinuous Movements of Fluid" Phil. Mag., 36, No. 4, 337-346.

Izumida, Y., Tamiya, S., and Kato, H., 1980, "The relationship between characteristics of partial cavitation and flow separation," Proc. 10th IAHR Symp., Tokyo, pp. 168-181.

Kjeldsen, M., Arndt, R.E.A. and Effertz, M., (1999) "Investigation of Unsteady Cavitation Phenomena" Proceedings of the 3rd ASME/JSME Fluids Engineering Conference, San Francisco, CA, July

Kirchhoff, G.(1869), "Zur Theorie Freier Flussigkeitsstrahlen", Jr. reine u. angew, Math., 70, 289-298.

Kiya, M.,, and Sasaki, K., 1985, "Structure of large-scale vortices and unsteady reverse flow in the reattaching zone of a turbulent separation bubble," Journal of Fluid Mechanics, vol. 154, pp. 463-491.

Kubota, A., Kato, H., Yamaguchi, H., and Maeda, M., "Unsteady structure measurement of cloud cavitation on a foil section using conditional sampling technique" J. Fluids Eng., 111, 204-210

MacCormack, R. W., (1969), " The effect of Viscosity in Hypervelocity Impact Cratering", AIAA Paper 69-354, Cincinnati, Ohio

Riabouchinsky, D. (1919), " On Steady Fluid Motion with Free Surface", Proc. London Math. Soc. 19, 206-215.

Song, C. S. (1965) " Two-dimensional Supercavitating Plate Oscillating Under a Free Surface", Journal of Ship Research, Vol. 9, No. 1, 40-55.

Song, C.C.S. and Yuan, M. (1988), " A weakly Compressible Flow Model and Rapid Convergence Methods", Journal of Fluids Engineering, Vol. 110, 441-445.

Song, C. C. S. (1996), " Compressibility boundary Layer Theory and its Significance in Computational Hydrodynamics", Journal of Hydrodynamics, Series B, Vol. 8, No.2, 92-101

Song, C.C.S. and Chen, X. (1996), " Compressibility Boundary Layer and Computation of Small Mach Number Flows", Hydrodynamics, Theory and Applications, Proc. 2nd International Conf. on Hydrodynamics, Hong Kong, 815-820.

Song, C.C.S., He, J., Zhou, F. and Wang, G. (1997), "Numerical Simulation of Cavitating and Non-cavitating Flows over a Hydrofoil," St. Anthony Falls Laboratory, Project Report No. 402, University of Minnesota

Tulin, M. P. (1958), " New Development in the Theory of Supercavitating Flows", Proc. Second Symp. on Naval Hydrodynamics, ONR/ACR-38, pp. 235-260.

Watanabe, S., Tsujimoto, Y., Franc, J.P., and Michel, J.M., (1998) "Linear Analyses of Cavitation Instabilities" Proceedings of Third International Symposium on Cavitation, Grenoble, France, April

Wu, T. Y. (1956), " A Free Streamline Theory for Two-dimensional Fully Cavitated Hydrofoils", Journal of Mathematics and Physics, 35, 236-265.

Ye, Z., Gopalan, S. and Katz, J. (1998) "On the Flow Structure and Vorticity Production due to Sheet Cavitation" Proceedings of 1998 ASME Fluids Engineering Division Summer Meeting, Paper No. FEDSAM98-5301

Zaman, K. B. M. Q., McKinzie, D. J., and Rumsey, C. L., 1989, "A natural low-frequency oscillation of the flow over an airfoil near stalling conditions," Journal of Fluid Mechanics, vol. 202, pp. 403-442.